Treatment with 5-aza-dC Induces Apoptotic PARP1-DNA Adducts

Kostantin Kiianitsa[1], Yinbo Zhang[1], and Nancy Maizels[1,2,3,*]
Departments of [1]Immunology and [2]Biochemistry
University of Washington, Seattle, WA 98195 USA
[3]Lead Contact
*correspondence: maizels@uw.edu

SUMMARY

5-aza-dC (5-aza-2'-deoxycytidine, clinically known as decitabine) is used to treat some hematopoietic malignancies, but its mechanism of action is not defined. Here we identify a role for covalent PARP1-DNA adducts in cell killing by 5-aza-dC. We demonstrate that covalent PARP1-DNA adducts can be recovered from cells treated with 5-aza-dC alone or in combination with a PARP catalytic inhibitor. PARP1-DNA adducts are predominately 89 kD in length, contain the cleaved PARP1 fragment that is a signature of apoptotic cells, and bear the terminal neo-epitope generated by caspase cleavage. Smaller PARP1-DNA adducts bearing the apoptotic neo-epitope were also detected, but not adducts containing full-length PARP1. DNA-adducted PARP1 fragments thus provide a biochemical link between drug-induced PARP1-DNA adduct formation and cell killing. They support a model in which 5-aza-dC causes DNA damage that recruits full-length PARP1, which forms covalent adducts that induce apoptosis, resulting in PARP1 cleavage and cell killing.

INTRODUCTION

The cytidine analog 5-aza-2'-deoxycytidine (5-aza-dC), known in the clinic as decitabine, is used to treat myelodysplasia syndrome (MDS) and acute myelogenous leukemia (AML) in patients who are unlikely to tolerate other drugs (Estey, 2013). Only a fraction of patients responds to 5-aza-dC and responses are typically limited in duration, so there is compelling motivation to understand the mechanism of cell killing by 5-aza-dC. 5-aza-dC is incorporated into DNA of replicating cells, where it may become a target for methylation by the maintenance DNA methyltransferase, DNMT1. Treatment with 5-aza-dC rapidly induces proteolysis and depletion of DNMT1, resulting in genome-wide loss of cytosine methylation and extensive epigenetic reprogramming (Ghoshal et al., 2005; Patel et al., 2010; Yu et al., 2018). The possibility that DNA demethylation might re-activate silenced tumor suppressor genes to limit cell proliferation provided the initial rationale for the use of 5-aza-dC in therapy of cancer, and 5-aza-dC is

commonly considered an “epigenetic” drug (Estey, 2013). However, attempts to correlate 5-aza-dC efficacy with reprogramming of specific genetic networks or pathways in AML cells have not been fruitful (Klco et al., 2013). A second mechanism by which 5-aza-dC may exert an anti-tumor effect is by affecting the course of the DNA methyltransferase reaction. In the course of methylation, a catalytic cysteine at the DNMT1 active site forms a covalent bond with the target cytosine (Fahy et al., 2012). If this cross-link is not reversed, the adducted DNMT1 polypeptide may block DNA replication and cause cell killing. However, the contribution of DNMT1-DNA adducts to cytotoxicity has not been systematically explored, due to the difficulty of isolating DNMT1-DNA adducts from 5-aza-dC-treated cells and the confounding effect of ongoing DNMT1 proteolysis.

DNA damage results from 5-aza-dC treatment, as evidenced by mutations and genomic instability in surviving cells (Juttermann et al., 1994; Jackson-Grusby et al., 1997; Palii et al., 2008; Maslov et al., 2012; Orta et al., 2013; Orta et al., 2014; Burgos-Moron et al., 2018). A multiprotein complex including not only DNMT1 but also PARP1 responds to damage requiring replicative repair (O'Hagan et al., 2011; Muvarak et al., 2016). PARP1 is a conserved, abundant and multifunctional eukaryotic enzyme that functions in the DNA damage response, DNA repair and transcriptional regulation [reviewed by (Caldecott, 2014; Pascal and Ellenberger, 2015; Ray Chaudhuri and Nussenzweig, 2017)]. PARP1 is activated by DNA damage including AP sites, 5’-dRP residues and single-strand breaks; and PARP1 regulates repair by catalyzing "PARylation", addition of poly(ADP-ribose) (PAR) chains synthesized from the coenzyme, NAD+ to itself and other factors. Small molecule inhibitors of PARP1 catalytic activity (“PARPi”) compete with NAD binding and prevent PARylation. PARPi are well-tolerated and effective drugs for the treatment of some tumors with repair deficiencies (Pommier et al., 2016; Lord and Ashworth, 2017; Nickoloff et al., 2017; Ray Chaudhuri and Nussenzweig, 2017; Ashworth and Lord, 2018; D'Andrea, 2018).

PARP1 forms covalent adducts in vitro with DNA substrates containing AP sites or 5’-dRP residues; and in cells treated with the alkylating agent, methyl methanesulfonate (Khodyreva et al., 2010; Prasad et al., 2014). Covalent adducts have considerable potential to contribute to cell killing, and some very potent drugs act by stabilizing covalent protein-DNA adducts formed by topoisomerases, including the camptothecin derivative, topotecan, which targets human topoisomerase 1; etoposide, which targets human topoisomerase 2; and fluoroquinolone antibiotics like ciprofloxacin, which target bacterial gyrase. The possible contribution of covalent PARP1-DNA adducts to cell killing has not been directly established, although PARP1 has long been recognized as part of the apoptotic program. In apoptotic cells, activated caspases 3,7 cleave 113 kD PARP1 to produce fragments of 24 and 89 kD (Kaufmann et al., 1993), and appearance of the 89 kD PARP1 fragment is a signature of ongoing apoptosis.

Here we show that PARP1 forms covalent DNA adducts in living cells treated with 5-aza-dC. Western blot analysis shows that these PARP1-DNA adducts are apoptotic: they are predominately 89 kD in length, composed of caspase 3,7-cleaved PARP1, and bear the terminal

neo-epitope generated by caspase 3,7 cleavage. Smaller PARP1-DNA adducts bearing this terminal neo-epitope can also be identified. Protein-DNA adducts are cytotoxic if not repaired prior to replication, so the caspase-cleaved PARP1-DNA adducts provide a biochemical link between PARP1-DNA adduct formation and induction of apoptosis. These results support a model in which DNA damage induced by 5-aza-dC treatment recruits full-length PARP1, which forms covalent adducts that promote cell killing and activate caspases that cleave adducted PARP1.

RESULTS

Depletion Analysis Implicates DNMT1 and PARP1 Adducts in Drug Sensitivity

Adduct formation was studied in two different cell types, K562 cells, an ENCODE cell line derived from a chronic myelogenous leukemia (CML) patient in blast crisis, which carry a null mutation in TP53; and GM639 cells, which derive from SV40-transformed primary human fibroblasts. Comparison of cell viability after 66 hr of 5-aza-dC treatment showed that GM639 cells were more resistant to this drug than K562 cells or two other human hematopoietic cell lines, HL-60 cells, a promyelocytic line derived from an AML patient; and CCRF-CEM cells, a T cell line derived from an acute lymphocytic leukemia (Figure S1). Because K562 and GM639 cells derive from different tissues, were transformed by different mechanisms, and differ in status of P53, a major regulator of apoptosis, they were anticipated to exhibit differences in drug sensitivity and apoptosis. Such differences were evident upon using flow cytometry to monitor changes in cell size and morphology caused by treatment with 5-aza-dC; with PARPi, which inhibits base excision repair of lesions caused by 5-aza-dC (Orta et al., 2014); or with both drugs, reported to synergize in cell killing (Muvarak et al., 2016). At 24 hr, the response to 5-aza-dC or PARPi alone (1 μM) was quite limited, but treatment with both 5-aza-dC and PARPi caused clear changes in both forward and side scatter in K562 and GM639 cells (Figure 1A). At 48 hr, K562 cells exhibited a modest response to 5-aza-dC and a greater response to PARPi or 5-aza-dC together with PARPi; and GM639 cells exhibited a robust response to these drugs as single agents or in combination. At 96 hr, a robust response was evident in K562 or GM639 cells treated with either drug alone, but cells could no longer be recovered from cells treated with both drugs. Assays of cell killing by dye exclusion showed that dead cells accumulated in cultures of K562 or GM639 cells treated with PARPi but not with 5-aza-dC alone; and that extended culture with 5-aza-dC was better-tolerated than extended culture with PARPi (Figure 1B). Cell recovery was reduced at late times (>96 hr), suggesting inhibition of cell division accompanied by ongoing lysis.

If adduct formation contributes to cell killing, then depletion of PARP1 is predicted to improve the viability of cells treated with drugs that promote formation of adducts. To test this, the effects of DNMT1 and PARP1 depletion were determined by treating cells with siRNAs shown to reduce protein levels (Figure S2), then culturing with 5-aza-dC and/or PARPi for four days before carrying out cell viability measurements. Dose response analysis showed that K562 cells were

sensitive to 5-aza-dC (EC_{50} = 0.1 μM), and that depletion of DNMT1 substantially reduced that sensitivity, increasing EC_{50} 10-fold, to 1 μM (Figure 1C, above). Depletion of PARP1 caused a modest increase in sensitivity, consistent with a role for PARP1 in repair of 5-aza-dC-induced damage (Orta et al., 2014). K562 cells were sensitive to PARPi (BMN-673; IC_{50} = 0.2 μM), and depletion of PARP1 reduced PARPi sensitivity 5-fold, to 1 μM, but depletion of DNMT1 did not affect PARPi sensitivity. 5-aza-C, the ribonucleotide analog of 5-aza-dC, also induces DNA demethylation and it is used to treat AML based on this activity. K562 cells were much less sensitive to 5-aza-C (EC_{50}=1 μM) than to 5-aza-dC, and DNMT1 depletion did not affect sensitivity (Figure S3), consistent with distinctly different effects of these two drugs on AML cell viability (Hollenbach et al., 2010). Synergy of 5-aza-dC and PARPi was evident, as previously reported for K562 cells and other cell types (Orta et al., 2014; Muvarak et al., 2016). GM639 cells were relatively insensitive to 5-aza-dC (Figures 1C, S1), but depletion of DNMT1 had a protective effect, while depletion of PARP1 caused a modest increase in sensitivity (Figure 1C, below), as with K562 cells. Depletion of PARP1 diminished sensitivity to PARPi, increasing IC_{50} 3-fold, from 1 to 3 μM. In contrast, depletion of PARP1 increased sensitivity to the topoisomerase 1 poison, topotecan (Figure S3), which causes DNA damage that depends upon PARP1 catalytic activity for repair (Maede et al., 2014; Murai et al., 2014). Synergy of 5-aza-dC and PARP1 in GM639 cells was clearly evident by viability analysis; and depletion of DNMT1 or PARP1 protected viability of cells treated with both drugs. Depletion analysis thus supports a possible role for DNMT1-DNA adducts in cell killing by 5-aza-dC, and for PARP1-DNA adducts in cell killing by PARPi.

Treatment with 5-aza-dC and/or PARPi Induces Apoptotic Cleavage of PARP1

In apoptotic cells, activated caspases 3,7 cleave 113 kD PARP1 between residues 214 and 215 (Kaufmann et al., 1993), generating an 89 kD fragment that bears a novel epitope for antigen recognition at its newly created N-terminal (Figure 2A). PARP1 cleavage was assayed in K562 and GM639 cells treated with either 5-aza-dC or PARPi alone (1 μM); or treated with 5-aza-dC for 48 hr followed by PARPi for 18 hr, a regimen that reflects the potential for 5-aza-dC incorporated over multiple cell divisions to enhance eventual damage [e.g. (Palii et al., 2008; Oz et al., 2014)]. Treatment of either K562 or GM639 cells with 5-aza-dC or PARPi induced PARP1 cleavage that generated the apoptotic 89 kD PARP1 fragment, as evidenced by Western blots of cell extracts probed with an affinity-purified murine mAb specific to the C-terminal catalytic domain (anti-cat-PARP1) that recognizes both 113 kD full-length and 89 kD caspase-cleaved PARP1 (Figure 2B). Reduced levels of 113 kD intact PARP1 accompanied by increased levels of 89 kD cleaved PARP1 were detected in K562 cells treated with 5-aza-dC for 66 hr; and in GM639 cells treated with 5-aza-dC followed by PARPi. Reduced levels of PARP1 were also detected in K562 cells treated with PARPi for 18 hr. PARP1 cleavage in populations of treated cells was confirmed by probing with a monoclonal antibody (mAb) specific for the neo-epitope created by caspase 3,7 cleavage (anti-cc-PARP1 mAb). This antibody detected a modest increase in 89 kD PARP1 levels

by 48 hr of 5-aza-dC treatment in K562 cells, and clearly increased levels in K562 cells treated with 5-aza-dC for 66 hr, and GM639 cells treated with 5-aza-dC followed by PARPi. DNMT1 levels were dramatically reduced upon 5-aza-dC treatment, as also documented in other cell types (Ghoshal et al., 2005; Yu et al., 2018). Surprisingly in K562 but not GM639 cells, DNMT1 levels began to recover at 66 hr; and treatment with PARPi alone or together with 5-aza-dC caused DNMT1 levels to increase. If stabilization of DNMT1 proves to be more general, it may provide a useful biomarker for the clinical response to PARPi.

To establish whether accumulation of cleaved PARP1 was evident in individual cells, aliquots of the same cultures analyzed above by Western blots were stained with a phycoerythrin (PE) conjugate of anti-cc-PARP1 mAb then analyzed by flow cytometry (Figure 2C). Less than 1% of cells scored positive in most samples. The exception was GM639 cells treated with 5-aza-dC followed by PARPi , where 3.3% of cells stained positive for cleaved PARP1. This sample also exhibited the most robust PARP1 cleavage upon Western blot analysis (Figure 2B).

RADAR/Slot Blots Identify PARP1-DNA Adducts Induced by Treatment with 5-aza-dC or PARPi

The RADAR extraction method developed in our laboratory (Kiianitsa and Maizels, 2013, 2014) was used to isolate protein-DNA adducts. In this approach, cells are lysed in a combination of chaotropes and detergent, which inhibits endogenous proteases and releases non-covalently bound proteins from DNA; nucleic acids and proteins bound covalently to DNA are recovered by isopropanol precipitation; nucleic acids are digested with Benzonase; and adducts are quantified by immunodetection (Figure 3A). RADAR/slot blots [e.g. (Kiianitsa and Maizels, 2013; Aldred et al., 2015; Quinones et al., 2015; Vaz et al., 2016; Mohni et al., 2019)] probed with a mAb that recognizes an epitope in the catalytic domain of PARP1 (anti-cat-PARP1) showed that PARP1-DNA adducts were induced by treatment of either K562 or GM639 cells with 5-aza-dC (Figure 3B). In K562 cells, PARP1-DNA adducts were induced 3-fold by 5-aza-dC, 2.5-fold by PARPi (olaparib) and 6-fold by 5-aza-dC and PARPi. In GM639 cells, PARP1 DNA adducts were induced 15-fold by treatment with 5-aza-dC alone, 21-fold by treatment with PARPi (BMN-673) alone, and 21-fold by treatment with PARPi and 5-aza-dC. RADAR/slot blots thus establish that covalent PARP1-DNA adducts are induced by treatment with 5-aza-dC and PARPi, alone or in combination.

A RADAR/slot blot probed with an anti-DNMT1 mAb showed that 5-aza-dC treatment of GM639 cells decreased the level of DNMT1-DNA adducts 5-fold relative to untreated cells; and that treatment with the proteasome inhibitor, bortezomib, caused a modest increase in DNMT1-DNA adduct levels (Figure 3C). These results are consistent with rapid proteolysis of DNMT1 in response to 5-aza-dC treatment [(Ghoshal et al., 2005; Patel et al., 2010; Yu et al., 2018); and Figure 2B].

RADAR/Western Blots Identify Apoptotic PARP1-DNA Adducts Induced by 5-aza-dC

To characterize adducted PARP1, RADAR extracts were analyzed by Western blots. A blot of RADAR extracts from K562 cells treated with 5-aza-dC, PARPi or both drugs was probed with rabbit polyclonal antibody raised against recombinant full-length human PARP1 (anti-fl-PARP1). This antibody recognized 113 kD PARP1 in whole cell extract from untreated cells but did not detect adducts containing 113 kD PARP1 in RADAR extracts of K562 cells (Figure 4A). A prominent polypeptide of 89 kD was detected, the size of caspase-cleaved PARP1, in RADAR extracts of cells treated with 5-aza-dC alone (48-66 hr) or with PARPi following 48 hr pre-treatment with 5-aza-dC (Figure 4A, lanes 4, 5, 10-12). Smaller polypeptides of 40-65 kD were also detected in the same samples. In RADAR extracts of cells treated with PARPi alone, no 89 kD adducts were detected, but faint signals were evident in the 40-65 kD size range (Figure 4A, lanes 6-9).

To determine whether the adducted 89 kD polypeptide carried the N-terminal neo-epitope generated upon caspase cleavage, RADAR/Western analysis was carried out on duplicate gels run in parallel, each of which contained RADAR extracts from K562 and GM639 cells. One sample on each gel consisted of nuclear extract from K562 cells treated with the apoptotic inducer staurosporine (STS; 1 μM,1 hr), to serve as an internal control for electrophoretic mobility and antibody specificity. The duplicate gels were transferred to nitrocellulose membranes, and one blot was probed with anti-cc-PARP1 mAb, to detect the neo-epitope generated upon PARP1 cleavage; and the other with anti-cat-PARP1, which recognizes an epitope in the PARP1 catalytic domain (Figure 4B). The anti-cc-PARP1 mAb detected 89 kD cleaved PARP1 but no other polypeptides in the control extract from STS-treated cells, verifying antibody specificity (Figure 4B, left, lane 1). The anti-cc-PARP1 mAb detected 89 kD cleaved PARP1 in the RADAR fraction of K562 cells treated with 5-aza-dC (Figure 4B, left, lane 8), confirming identification of the 89 kD polypeptide detected by anti-fl-PARP1 (Figure 4A) as the PARP1 cleavage product. In samples from GM639 cells treated with 5-aza-dC alone or 5-aza-dC and PARPi, the anti-cc-PARP1 mAb identified 89 kD cleaved PARP1 along with smaller polypeptides of 40-65 kD that bear the neo-epitope generated upon caspase 3,7 cleavage (Figure 4B, left, lanes 3, 4, 6).

Probing the duplicate blot with anti-cat-PARP1, which recognizes the catalytic domain, identified both full-length 113 kD and cleaved 89 kD PARP1 polypeptides in the control sample from STS-treated cells (Figure 4B, right, lane 1). This mAb identified the 89 kD PARP1 cleavage product and smaller polypeptides among adducts isolated from cells treated with 5-aza-dC and 5-aza-dC followed by PARPi (Figure 4B, right, lanes 3, 4, 6), but did not detect adducts containing full-length PARP1 in any samples. In RADAR extracts of GM639 cells treated with PARPi alone, 89 kD cleaved PARP1 was not detected, but smaller polypeptides which exhibited essentially identical migration patterns on blots probed with anti-cc-PARP1 and anti-cat-PARP1 (Figure 4B, compare left and right blots, lane 5). The N-terminal neo-epitope generated upon caspase cleavage must be intact for recognition by the anti-cc-PARP1 mAb, so these smaller polypeptides appear to be generated by proteolysis of the C-terminal of caspase-cleaved PARP1.

To ask if DNMT1-DNA adducts could be detected by RADAR/Western, RADAR extracts prepared from cultures of GM639 cells in three different experiments were resolved on a blot that was first probed with the murine anti-cc-PARP1 mAb, to confirm induction of PARP1-DNA adducts (Figure 4C, left). The blot was washed but not stripped of the anti-PARP1 mAb, then probed with a rabbit anti-DNMT1 mAb that recognizes a C-terminal region of DNMT1 close to the site of adduct formation (Figure 4C, right). The anti-DNMT1 mAb detected intact DNMT1 (180 kD) and minor proteolytic products in the control lane (whole cell extract), but this antibody did not detect a species of 180 kD or smaller in any of the RADAR extracts. These results are consistent with proteolysis of both free and DNA-adducted DNMT1 in response to 5-aza-dC treatment reported by others (Ghoshal et al., 2005; Patel et al., 2010; Yu et al., 2018); and confirmed by other results reported here (Figures 2B, 3C).

DISCUSSION

The analysis reported here shows that treatment with 5-aza-dC, alone or in combination with PARPi, induces PARP1-DNA covalent adducts, which are targeted for cleavage by apoptotic caspases. Considerable effort has been devoted to understanding the mechanism of action of 5-aza-dC, but this possibility had not been previously suggested. Although initially surprising, the ability of single agent 5-aza-dC to induce PARP1-DNA adducts is readily explained in the context of the known activities of 5-aza-dC, DNMT1 and PARP1. Incorporation of 5-aza-dC can induce DNA damage, either directly or as a result of aberrant repair of the normally transient covalent DNA adducts formed by DNMT1 (Juttermann et al., 1994; Jackson-Grusby et al., 1997; Palii et al., 2008; Maslov et al., 2012; Orta et al., 2013; Orta et al., 2014; Jeltsch and Jurkowska, 2016; Burgos-Moron et al., 2018). Depletion of DNMT1 protected K562 and GM369 cells from 5-aza-dC, indicating that DNMT1 adducts contribute significantly to 5-aza-dC cytotoxicity in both cell types. PARP1 catalytic activity appears to be important for repair of 5-aza-dC-induced DNA damage because PARP1 depletion moderately increased sensitivity to 5-aza-dC. This leads to a working model in which DNMT1-DNA adducts formed in response to 5-aza-dC treatment subsequently rely on PARP1 for repair (Figure 5).

Protein-DNA adducts are cytotoxic if not repaired prior to cell division. Adduct formation and initiation of apoptosis must therefore occur after the final cell cycle has begun, and the structure of recovered adducts will provide a record of events that occurred in the time between adduct formation and cell death. No full-length 113 kD PARP1 DNA adducts were identified; but apoptotic PARP1-DNA adducts bearing the neo-epitope characteristic of cleavage by activated caspases 3,7 were readily detected. Apoptotic 89 kD PARP1-DNA adducts were further degraded by proteases that targeted the C-terminal region. This may be due to activities of proteases specialized for repair of DNA-protein adducts, such as SPRTN (Vaz et al., 2016; Stingele et al., 2017). Mutational analysis has mapped the region essential for PARP1 interaction with chromatin

and PARPi sensitivity to the two N-terminal ZNF motifs, a region lacking from the 89 kD cleavage PARP1 fragment (Pettitt et al., 2018). Apoptotic cleavage thus separates the region critical for interaction with chromatin from the region that forms adducts (Figure 2A) and is predicted to impair DNA binding necessary for PARP1-DNA adduct formation. Recovery of adducts composed of caspase-cleaved PARP1 therefore supports a model in which adducts formed by full-length PARP1 cause replication arrest which induces apoptosis that results in adduct cleavage, and apoptotic PARP1-DNA adducts provide a biochemical link between induction of PARP1-DNA adducts and cell killing by treatment with 5-aza-dC.

The number of positions substituted with 5-aza-dC increases over the course of continuous culture with drug (Palii et al., 2008; Oz et al., 2014), which will cause an increase in the number of sites per cell which may recruit PARP1 for repair. This may account for the increased PARP1-DNA adduct recovery per cell late in the course of treatment with 5-aza-dC (48-66 hr; Figure 4C), as may cell cycle arrest in cells with unrepaired adducts. The number of PARP1 adducts present in a cell can be estimated by comparing the signals in lanes containing a RADAR sample and whole cell extract. In the experiment shown in Figure 4A, treated samples were derived from 300-fold more cells than untreated samples (input of $3x10^6$ cell equivalents relative to 10^4 cell equivalents), and the signal from cells treated with 5-aza-dC (1 μM) for 66 hr (lane 5) was approximately 8-fold below that from whole cell extract (lane 1). Assuming that the abundance of PARP1 is 10^6 molecules/cell, then approximately 1/8x300=1/2400 of those molecules, or 400 PARP1 molecules/cell were recovered as 89 kD adducts, a level likely to exceed the level of adducts necessary for cell killing. This suggests that it may be possible to activate PARP1-DNA adduct mediated cell killing by administration of 5-aza-dC at low doses over extended times.

Apoptotic PARP1-DNA adducts of similar structure were identified following 5-aza-dC treatment in both K562 hematopoietic cells and GM639 transformed fibroblasts, which exhibit distinct responses to drug treatment and induction of apoptosis (Figures 1,2). Cell killing by PARP1-DNA adducts is therefore likely to generalize to additional cell types and contexts. This suggests that it may be possible to extend therapeutic application of 5-aza-dC to solid tumors. A recent study described 5-aza-dC-sensitivity of patient-derived xenograft tissue from triple-negative breast cancers (Yu et al., 2018). Notably, this study documented a positive correlation between sensitivity and DNMT1 levels, as would be predicted if the pathway for sensitivity involved protein-DNA adduct formation.

PARPi also induced PARP1-DNA adducts, which were evident in RADAR/slot blots of K562 or GM639 cells treated with single agent PARPi (Figure 3B). Depletion analysis presented here (Figure 1C) and evidence that deletion or ablation of PARP1 protects from PARPi sensitivity (Murai et al., 2012; Pettitt et al., 2013; Pettitt et al., 2018; Thomas et al., 2018) further supports the ability of PARPi to induce cytotoxic PARP1-DNA adducts. The fact that only modest (if any) induction of adducts by PARPi was evident in Western blots suggests that, in cells treated with PARPi alone,

PARP1-DNA adducts may undergo proteolysis that generates fragments of heterogeneous size that are not detectable as bands of discrete sizes in Western blots.

PARPi are well-tolerated and effective drugs for the treatment of cancer, but currently their use is largely restricted to cancers with germline deficiencies in BRCA1/2. PARPi's were first used to treat tumors with defects in homology dependent repair (HDR) resulting from BRCA1 or BRCA2-deficiency (Bryant et al., 2005; Farmer et al., 2005). The mechanism initially proposed to explain cell killing by PARPi was that inhibition of PARP catalytic activity prevents repair of DNA nicks, allowing them to accumulate and become converted to replicative DSBs that depend upon HDR. The identification of apoptotic PARP1-DNA adducts reported here suggests that it may be worthwhile to explore other mechanisms of cell killing by PARPi, as this may enable the extension of PARPi therapy to new contexts.

METHODS

Cell culture, viability assays, siRNA depletion and drug treatment

K562, HL-60 and CCRF-CEM cells were obtained from ATCC and cultured in RPMI medium with 10% fetal calf serum. GM639 cells, an SV40-transformed human fibroblast line (gift of Dr. Ray Monnat, University of Washington), were cultured in DMEM medium with 10% fetal calf serum. Bortezomib and olaparib were from LC Laboratories and talazoparib (BMN-673) from ApexBio. 5-aza-dC was obtained from Calbiochem/EMD Millipore; 5-aza-cytidine from Sigma; and topotecan from Enzo Life Sciences; Ambion Silencer® Select siRNAs to PARP1 (#4427038; s1099), DNMT1 (#4427038; s4216) and Negative Control No. 2 siRNA (siNT2, #4390846) were purchased from Thermo Fisher. siRNA nucleofection of K562 cells was carried out according to the protocol provided by Lonza. siRNA transfection of GM639 cells was performed using Lipofectamine RNAiMax (Invitrogen) according to the manufacturer's protocol. siRNAs were verified to reduce protein levels in K562 and GM639 cells by Western blots (Figure S2). Drug response was assayed at 48-72 hr after initiation of siRNA treatment. Cell viability was measured using the CellTiter-Glo® assay (Promega). Control extracts that contained both 113 kD PARP1 and the 89 kD PARP1 cleavage product were generated from cells treated with staurosporin (STS; EMD Millipore; 1 μM, 1 hr).

Antibodies

Primary antibodies used for Western blot analyses were: rabbit polyclonal antibodies raised against recombinant full-length PARP1 (anti-fl-PARP1, ALX-210-302-R100, Enzo Life Sciences; 1:4000 dilution); clone 7D3-6, an affinity-purified mouse monoclonal antibody (mAb) that recognizes an epitope in the C-terminal NAD binding and catalytic domain of human PARP1 (anti-cat-PARP1, #556493, BD Biosciences; 1:1000 dilution); clone F21-852 mouse mAb specific for the neo-epitope generated at the N-terminal of the 89 kD PARP1 fragment formed after cleavage by

apoptotic caspases between Asp214/Gly215 (anti-cc-PARP1, #552596, BD Biosciences, 1:2000 dilution); a rabbit mAb that recognizes an epitope between residue 1500-1600 near the C-terminal of DNMT1 (anti-DNMT1, ab188453, Abcam; 1:1000 dilution); and clone DM1A mouse mAb that recognizes α-tubulin (anti-tubulin, ab7291, Abcam; 1:4000 dilution). Secondary detection was carried out using HRP-conjugated goat anti-mouse IgG or donkey anti-rabbit IgG (BioLegend, #405306 and #406401, respectively; 1:5000 dilution). Immune complexes were visualized using the ECL system (Pierce).

A phycoerythrin (PE)-conjugated derivative of the anti-cc-PARP monoclonal (#552933, BD Biosciences) was used for detection of intracellular cleaved PARP1 by flow cytometry.

Flow cytometry

Approximately $1x10^6$ cells were harvested by either pipetting (K562) or trypsinization (0.05%) then washed twice with cold PBS. Samples were resuspended in 200 µl and analyzed by flow cytometry on a BD LSR II instrument, set to record 50,000 cells per sample. Linear area of width and height of the forward scatter (FSC) and side scatter (SSC) (linear) were recorded. To assay viability by dye exclusion, cells were stained in 250 µl of Fixable Viability Dye eFluor™ 450 (Invitrogen™; 1:1000 dilution in PBS) for 15 min on ice, then washed prior to resuspension and flow cytometry. To detect cells containing caspase-cleaved PARP1, cells were fixed and permeabilized with 500 µl of 1x Foxp3 /Transcription Factor Fixation/Permeabilization solution (Invitrogen™) for 30 min at room temperature; washed twice with 500 µl of 1x Foxp3/Transcription Factor permeabilization buffer (Invitrogen); stained with 250 µl of PE-conjugated anti-cc-PARP1 in the same buffer (#552933, BD Biosciences; 1:100 dilution) for one hr at room temperature; washed once in 1 ml; and resuspended in 200 µl for flow cytometry. Data were analyzed using FlowJo software (version 9.6). The linear area of FSC and SSC were gated relative to untreated cells to represent the relative cell size and internal complexity. Fluorescent channel Pacific Blue was collected in log area to measure cells labeled with viability dye (dead cells), and fractions of dead cells were gated by using the histogram of log area of positive Pacific Blue signal of the untreated whole cell population, compared to the histogram of unstained cells. Fluorescent channel PE was collected in log area to measure cells labeled with PE-conjugated anti-cc-PARP. Fractions of cells containing cleaved PARP1 were gated by PE positive among SSC, using unstained cells as a reference.

Nucleic acid and protein quantification

DNA and RNA were quantified using DNA/RNA specific fluorescent detection kits (Qubit, Invitrogen). Total protein was measured using BCA detection kit (Pierce).

RADAR/Western analysis

DNA-protein adducts were purified for RADAR/Western analysis using an adaptation of the RADAR (rapid approach to DNA adduct recovery) fractionation protocol in which cells are directly

lysed in the presence of chaotrope and detergents, after which nucleic acids including protein-DNA adducts are separated from total protein by precipitation in alcohol (Kiianitsa and Maizels, 2013, 2014). For recovery of adducts from GM639 cells, 10-15 x 10^6 cells were harvested by centrifugation and washed in PBS prior to fractionation; up to 4-fold more starting material was used for recovery of adducts from K562 cells. PARP1 is an abundant protein (1-2x10^6 molecules/cell). To reduce potential background of non-covalently bound PARP1, we introduced two additional steps into the fractionation procedure. (1) Cytoplasm, including rRNA and up to 75% of total protein was eliminated by quick lysis in 1 ml MPER reagent (Pierce/Thermo Fisher) supplemented with Halt protease inhibitor cocktail (Thermo Fisher) and 1 mM DTT. Homogenization was performed by 8-10 pipet strokes. After 2 min centrifugation at maximal speed, nuclear pellets (MPER-P) were collected by brief centrifugation. The MPER-P fraction includes essentially all genomic DNA, as less than 1% DNA was detected in the supernatant (MPER-S). Western blot analysis showed that PARP1, DNMT1, Top1 and histone H3 were exclusively in the MPER-P fraction. (2) The MPER-P pellets were promptly lysed in 400 µl of RADAR lysis buffer (LS1), consisting of 5 M guanidinium isothiocyanate (GTC), 2% Sarkosyl, 10 mg/ml DTT, 20 mM EDTA, 20 mM Tris-HCl (pH 8.0) and 0.1 M sodium acetate (pH 5.3), and adjusted to final pH 6.5 with NaOH. Lysates were transferred to polystyrene tubes (Evergreen) and sonicated on ice using a cup horn device (QSONICA) with ten 30 sec pulses at amplitude 100, and 60 sec cool-off time between pulses. Sonication yielded an average DNA size of 500 bp. After sonication, lysates were mixed with 80 µl 12 M LiCl (final concentration 2M LiCl, 4.16 M GTC) and incubated for 10 min at 37ºC on the Thermoshaker, then cleared by 10 min centrifugation at 14,000 rpm at room temperature prior to conservative recovery of the supernatant. Lysates (volume approximately 450 µl) were transferred to new tubes, mixed with an equal volume of isopropanol; and nucleic acids were precipitated by 5 min centrifugation at 14,000 rpm at room temperature. Silica was not included to assist DNA precipitation as it had an adverse effect on purity when processing high numbers (more than 10^7) of cells. Pellets were washed thrice by vortexing with 1 ml 75% ethanol, followed by 2 min centrifugation. Nucleic acid pellets were dissolved in 100-200 µl of freshly prepared 8 mM NaOH by 30-60 min shaking on a Thermomixer at 37ºC. pH of eluates was neutralized by addition of 1 M HEPES to a final concentration of 10 mM. The resulting samples contained mostly genomic DNA and some nuclear RNA. The DNA/protein weight ratio was 100:3 or higher, comparable to adducts prepared by ultracentrifugation in a CsCl gradient.

Prior to gel electrophoresis, samples containing 10-30 µg genomic DNA each were treated with Benzonase nuclease (EMD Millipore; 0.5 units per µg DNA) in the presence of 2 mM magnesium chloride for 30 min at 37ºC to digest DNA. Completeness of nuclease digestion was verified by Qubit assays. Samples were resolved on precast 4-12% gradient protein gels (Bolt, Invitrogen), transferred to nitrocellulose membranes (0.45 µM pore, Invitrogen) and probed with

antibodies in PBST buffer (PBS containing 0.05% Tween 20) with 0.5% alkali-soluble casein (Novagen) as blocking agent.

ACKNOWLEDGMENTS

This research was funded by P01 CA077852 and R21 CA194876 from the US National Institutes of Health.

AUTHOR CONTRIBUTIONS

Conceptualization: K.K., Y.Z. and N.M.; Investigation: K.K. and Y.Z.; Writing: K.K., Y.Z. and N.M.; Funding Acquisition: N.M.

DECLARATION OF INTERESTS

The authors declare no competing interests.

REFERENCES

Aldred, K.J., Schwanz, H.A., Li, G., Williamson, B.H., McPherson, S.A., Turnbough, C.L., Jr., Kerns, R.J., and Osheroff, N. (2015). Activity of quinolone CP-115,955 against bacterial and human type II topoisomerases is mediated by different interactions. Biochemistry *54*, 1278-1286.

Ashworth, A., and Lord, C.J. (2018). Synthetic lethal therapies for cancer: what's next after PARP inhibitors? Nat Rev Clin Oncol *15*, 564-576.

Bryant, H.E., Schultz, N., Thomas, H.D., Parker, K.M., Flower, D., Lopez, E., Kyle, S., Meuth, M., Curtin, N.J., and Helleday, T. (2005). Specific killing of BRCA2-deficient tumours with inhibitors of poly(ADP-ribose) polymerase. Nature *434*, 913-917.

Burgos-Moron, E., Calderon-Montano, J.M., Pastor, N., Hoglund, A., Ruiz-Castizo, A., Dominguez, I., Lopez-Lazaro, M., Hajji, N., Helleday, T., Mateos, S.*, et al.* (2018). The Cockayne syndrome protein B is involved in the repair of 5-AZA-2'-deoxycytidine-induced DNA lesions. Oncotarget *9*, 35069-35084.

Caldecott, K.W. (2014). Protein ADP-ribosylation and the cellular response to DNA strand breaks. DNA Repair (Amst) *19*, 108-113.

D'Andrea, A.D. (2018). Mechanisms of PARP inhibitor sensitivity and resistance. DNA Repair (Amst).

Estey, E.H. (2013). Epigenetics in clinical practice: the examples of azacitidine and decitabine in myelodysplasia and acute myeloid leukemia. Leukemia *27*, 1803-1812.

Fahy, J., Jeltsch, A., and Arimondo, P.B. (2012). DNA methyltransferase inhibitors in cancer: a chemical and therapeutic patent overview and selected clinical studies. Expert Opin Ther Pat *22*, 1427-1442.

Farmer, H., McCabe, N., Lord, C.J., Tutt, A.N., Johnson, D.A., Richardson, T.B., Santarosa, M., Dillon, K.J., Hickson, I., Knights, C.*, et al.* (2005). Targeting the DNA repair defect in BRCA mutant cells as a therapeutic strategy. Nature *434*, 917-921.

Ghoshal, K., Datta, J., Majumder, S., Bai, S., Kutay, H., Motiwala, T., and Jacob, S.T. (2005). 5-Aza-deoxycytidine induces selective degradation of DNA methyltransferase 1 by a proteasomal pathway that requires the KEN box, bromo-adjacent homology domain, and nuclear localization signal. Mol Cell Biol *25*, 4727-4741.

Hollenbach, P.W., Nguyen, A.N., Brady, H., Williams, M., Ning, Y., Richard, N., Krushel, L., Aukerman, S.L., Heise, C., and MacBeth, K.J. (2010). A comparison of azacitidine and decitabine activities in acute myeloid leukemia cell lines. PLoS One *5*, e9001.

Jackson-Grusby, L., Laird, P.W., Magge, S.N., Moeller, B.J., and Jaenisch, R. (1997). Mutagenicity of 5-aza-2'-deoxycytidine is mediated by the mammalian DNA methyltransferase. Proc Natl Acad Sci U S A *94*, 4681-4685.

Jeltsch, A., and Jurkowska, R.Z. (2016). Allosteric control of mammalian DNA methyltransferases - a new regulatory paradigm. Nucleic Acids Res *44*, 8556-8575.

Juttermann, R., Li, E., and Jaenisch, R. (1994). Toxicity of 5-aza-2'-deoxycytidine to mammalian cells is mediated primarily by covalent trapping of DNA methyltransferase rather than DNA demethylation. Proc Natl Acad Sci U S A *91*, 11797-11801.

Kaufmann, S.H., Desnoyers, S., Ottaviano, Y., Davidson, N.E., and Poirier, G.G. (1993). Specific proteolytic cleavage of poly(ADP-ribose) polymerase: an early marker of chemotherapy-induced apoptosis. Cancer Res *53*, 3976-3985.

Khodyreva, S.N., Prasad, R., Ilina, E.S., Sukhanova, M.V., Kutuzov, M.M., Liu, Y., Hou, E.W., Wilson, S.H., and Lavrik, O.I. (2010). Apurinic/apyrimidinic (AP) site recognition by the 5'-dRP/AP lyase in poly(ADP-ribose) polymerase-1 (PARP-1). Proc Natl Acad Sci U S A *107*, 22090-22095.

Kiianitsa, K., and Maizels, N. (2013). A rapid and sensitive assay for DNA-protein covalent complexes in living cells. Nucleic Acids Res *41*, e104.

Kiianitsa, K., and Maizels, N. (2014). Ultrasensitive isolation, identification and quantification of DNA-protein adducts by ELISA-based RADAR assay. Nucleic Acids Res, In press.

Klco, J.M., Spencer, D.H., Lamprecht, T.L., Sarkaria, S.M., Wylie, T., Magrini, V., Hundal, J., Walker, J., Varghese, N., Erdmann-Gilmore, P.*, et al.* (2013). Genomic impact of transient low-dose decitabine treatment on primary AML cells. Blood *121*, 1633-1643.

Langelier, M.F., and Pascal, J.M. (2013). PARP-1 mechanism for coupling DNA damage detection to poly(ADP-ribose) synthesis. Curr Opin Struct Biol *23*, 134-143.

Lord, C.J., and Ashworth, A. (2017). PARP inhibitors: Synthetic lethality in the clinic. Science *355*, 1152-1158.

Maede, Y., Shimizu, H., Fukushima, T., Kogame, T., Nakamura, T., Miki, T., Takeda, S., Pommier, Y., and Murai, J. (2014). Differential and common DNA repair pathways for topoisomerase I-

and II-targeted drugs in a genetic DT40 repair cell screen panel. Mol Cancer Ther *13*, 214-220.

Maslov, A.Y., Lee, M., Gundry, M., Gravina, S., Strogonova, N., Tazearslan, C., Bendebury, A., Suh, Y., and Vijg, J. (2012). 5-aza-2'-deoxycytidine-induced genome rearrangements are mediated by DNMT1. Oncogene *31*, 5172-5179.

Mohni, K.N., Wessel, S.R., Zhao, R., Wojciechowski, A.C., Luzwick, J.W., Layden, H., Eichman, B.F., Thompson, P.S., Mehta, K.P.M., and Cortez, D. (2019). HMCES Maintains Genome Integrity by Shielding Abasic Sites in Single-Strand DNA. Cell *176*, 144-153 e113.

Murai, J., Huang, S.Y., Das, B.B., Renaud, A., Zhang, Y., Doroshow, J.H., Ji, J., Takeda, S., and Pommier, Y. (2012). Trapping of PARP1 and PARP2 by Clinical PARP Inhibitors. Cancer Res *72*, 5588-5599.

Murai, J., Zhang, Y., Morris, J., Ji, J., Takeda, S., Doroshow, J.H., and Pommier, Y. (2014). Rationale for poly(ADP-ribose) polymerase (PARP) inhibitors in combination therapy with camptothecins or temozolomide based on PARP trapping versus catalytic inhibition. J Pharmacol Exp Ther *349*, 408-416.

Muvarak, N.E., Chowdhury, K., Xia, L., Robert, C., Choi, E.Y., Cai, Y., Bellani, M., Zou, Y., Singh, Z.N., Duong, V.H.*, et al.* (2016). Enhancing the Cytotoxic Effects of PARP Inhibitors with DNA Demethylating Agents - A Potential Therapy for Cancer. Cancer Cell *30*, 637-650.

Nickoloff, J.A., Jones, D., Lee, S.H., Williamson, E.A., and Hromas, R. (2017). Drugging the Cancers Addicted to DNA Repair. J Natl Cancer Inst *109*.

O'Hagan, H.M., Wang, W., Sen, S., Destefano Shields, C., Lee, S.S., Zhang, Y.W., Clements, E.G., Cai, Y., Van Neste, L., Easwaran, H.*, et al.* (2011). Oxidative damage targets complexes containing DNA methyltransferases, SIRT1, and polycomb members to promoter CpG Islands. Cancer Cell *20*, 606-619.

Orta, M.L., Calderon-Montano, J.M., Dominguez, I., Pastor, N., Burgos-Moron, E., Lopez-Lazaro, M., Cortes, F., Mateos, S., and Helleday, T. (2013). 5-Aza-2'-deoxycytidine causes replication lesions that require Fanconi anemia-dependent homologous recombination for repair. Nucleic Acids Res.

Orta, M.L., Hoglund, A., Calderon-Montano, J.M., Dominguez, I., Burgos-Moron, E., Visnes, T., Pastor, N., Strom, C., Lopez-lazaro, M., and Helleday, T. (2014). The PARP inhibitor Olaparib disrupts base excision repair of 5-aza-2'-deoxycytidine lesions. Nucleic Acids Res *42*, 9108-9120.

Oz, S., Raddatz, G., Rius, M., Blagitko-Dorfs, N., Lubbert, M., Maercker, C., and Lyko, F. (2014). Quantitative determination of decitabine incorporation into DNA and its effect on mutation rates in human cancer cells. Nucleic Acids Res *42*, e152.

Palii, S.S., Van Emburgh, B.O., Sankpal, U.T., Brown, K.D., and Robertson, K.D. (2008). DNA methylation inhibitor 5-Aza-2'-deoxycytidine induces reversible genome-wide DNA damage that is distinctly influenced by DNA methyltransferases 1 and 3B. Mol Cell Biol *28*, 752-771.

Pascal, J.M., and Ellenberger, T. (2015). The rise and fall of poly(ADP-ribose): An enzymatic perspective. DNA Repair (Amst) *32*, 10-16.

Patel, K., Dickson, J., Din, S., Macleod, K., Jodrell, D., and Ramsahoye, B. (2010). Targeting of 5-aza-2'-deoxycytidine residues by chromatin-associated DNMT1 induces proteasomal degradation of the free enzyme. Nucleic Acids Res *38*, 4313-4324.

Pettitt, S.J., Krastev, D.B., Brandsma, I., Drean, A., Song, F., Aleksandrov, R., Harrell, M.I., Menon, M., Brough, R., Campbell, J.*, et al.* (2018). Genome-wide and high-density CRISPR-Cas9 screens identify point mutations in PARP1 causing PARP inhibitor resistance. Nat Commun *9*, 1849.

Pettitt, S.J., Rehman, F.L., Bajrami, I., Brough, R., Wallberg, F., Kozarewa, I., Fenwick, K., Assiotis, I., Chen, L., Campbell, J.*, et al.* (2013). A genetic screen using the PiggyBac transposon in haploid cells identifies Parp1 as a mediator of olaparib toxicity. PLoS One *8*, e61520.

Pommier, Y., O'Connor, M.J., and de Bono, J. (2016). Laying a trap to kill cancer cells: PARP inhibitors and their mechanisms of action. Sci Transl Med *8*, 362ps317.

Prasad, R., Horton, J.K., Chastain, P.D., 2nd, Gassman, N.R., Freudenthal, B.D., Hou, E.W., and Wilson, S.H. (2014). Suicidal cross-linking of PARP-1 to AP site intermediates in cells undergoing base excision repair. Nucleic Acids Res *42*, 6337-6351.

Quinones, J.L., Thapar, U., Yu, K., Fang, Q., Sobol, R.W., and Demple, B. (2015). Enzyme mechanism-based, oxidative DNA-protein cross-links formed with DNA polymerase beta in vivo. Proc Natl Acad Sci U S A *112*, 8602-8607.

Ray Chaudhuri, A., and Nussenzweig, A. (2017). The multifaceted roles of PARP1 in DNA repair and chromatin remodelling. Nat Rev Mol Cell Biol *18*, 610-621.

Smith, S. (2001). The world according to PARP. Trends Biochem Sci *26*, 174-179.

Soldani, C., and Scovassi, A.I. (2002). Poly(ADP-ribose) polymerase-1 cleavage during apoptosis: an update. Apoptosis *7*, 321-328.

Stingele, J., Bellelli, R., and Boulton, S.J. (2017). Mechanisms of DNA-protein crosslink repair. Nat Rev Mol Cell Biol *18*, 563-573.

Thomas, A., Murai, J., and Pommier, Y. (2018). The evolving landscape of predictive biomarkers of response to PARP inhibitors. J Clin Invest *128*, 1727-1730.

Vaz, B., Popovic, M., Newman, J.A., Fielden, J., Aitkenhead, H., Halder, S., Singh, A.N., Vendrell, I., Fischer, R., Torrecilla, I.*, et al.* (2016). Metalloprotease SPRTN/DVC1 Orchestrates Replication-Coupled DNA-Protein Crosslink Repair. Mol Cell *64*, 704-719.

Yu, J., Qin, B., Moyer, A.M., Nowsheen, S., Liu, T., Qin, S., Zhuang, Y., Liu, D., Lu, S.W., Kalari, K.R.*, et al.* (2018). DNA methyltransferase expression in triple-negative breast cancer predicts sensitivity to decitabine. J Clin Invest *128*, 2376-2388.

FIGURE LEGENDS

Figure 1. Depletion Analysis Implicates DNMT1 and PARP1 Adducts in Drug Sensitivity

(A) Flow cytometry analyses of forward scatter (x-axis) and side scatter (y-axis) in populations of K562 and GM639 cells treated with 1 μM 5-aza-dC, PARPi (BMN-673) or both for 0, 24, 48 or 96 hr, as indicated. Cells were gated by FSC-A and SSC-A comparison to untreated cells. Percent of cells outside the gate indicated in each scatter plot.

(B) Quantification of results of eFluor™ 450 Fixable Viability Dye (Invitrogen™) dye exclusion assays by flow cytometry of live K562 or GM632 cells treated with 1 μM 5-aza-dC or PARPi (BMN-673, BMN) for 0-96 hr.

(C) Effect of depletion of DNMT1 and/or PARP1 on the response of K562 and GM639 cells to drug treatment quantified by CellTiter-Glo® viability assays. Cells were treated for 48 hr with siDNMT1, siPARP1, or non-specific siRNA, siNT2; then cultured for 96 hr with drugs as indicated, including: 5-aza-dC (DAC; 0-4 μM); PARPi (BMN; 0-4 μM); or PARPi (BMN, 0-4 μM) in the presence of 250 nM DAC. Depletion was verified by Western blot (Figure S2).

Figure 2. Induction of Apoptosis and Apoptotic Cleavage of PARP1

(A) The diagram shows 113 kD PARP1, the three zinc finger motifs (FI, F2 and F3) in the DNA binding domain (DBD), a region essential for formation of covalent PARP1-DNA complexes in vitro (adducts) ref. Prasad et al, 2014, the BRCT domain, WGR repeats and NAD binding and catalytic domain (Smith, 2001; Soldani and Scovassi, 2002; Langelier and Pascal, 2013). In apoptotic cells, activated caspases 3/7 cleave PARP1 between residues Asp214 and Glu215 to generate 24 kD and 89 kD fragments from the N- and C-termini, respectively. This creates a neo-epitope at the new N-terminal of the larger cleaved PARP1 fragment.

(B) Western blot analyses of extracts of K562 or GM639 cells which were not treated (NT) or treated with 1 μM 5-aza-dC (D) or 1 μM PARPi (BMN-673, B) for indicated times; or treated with 5-aza-dC for 48 hr prior to addition of PARPi and further culture for 18 hr (D/B 48/18 hr). Blots were probed with mAbs specific for the neo-epitope on caspase-cleaved PARP1 (anti-cc-PARP1); the PARP1 catalytic domain (anti-cat-PARP1); DNMT1; or anti-tubulin.

(C) Representative analyses by flow cytometry of the fraction of cells expressing the neo-epitope characteristic of caspase-cleaved PARP1 following drug treatment. Aliquots of cells analyzed in Panel B were stained with PE-conjugated anti-cc-PARP1. Cells were gated to remove debris and doublets. Frequencies of cells stained by antibody shown in boxes.

Figure 3. RADAR/Slot Blots Identify PARP1-DNA Adducts Induced by 5-aza-dC

(A) Outline of recovery of DNA-protein adducts by RADAR fractionation. Proteins, colored circles. Drug, yellow pentagons.

(B) Analysis of induction of PARP1-DNA adducts in K562 or GM639 cells by RADAR/slot blots probed with anti-CAT-PARP1 mAb. Cells were not treated (NT) or treated for 40 hr with 5-aza-dC (DAC; 1 μM) and/or PARPi (olaparib; OLA, 1 μM; or BMN-673; BMN, 1 μM). For each cell type, lanes from slot blots are shown on the left and signal normalized to untreated cells on the right, with a dotted line indicating this base-line.
(C) Analysis of induction of DNMT1-DNA adducts in GM639 cells by RADAR/slot blot probed with anti-DNMT1 mAb. Cells were not treated (NT) or treated for 6 hr with 5-aza-dC (DAC; 5 μM) and/or the proteasome inhibitor, bortezomib (BTZ) (260 nM). Lanes from slot blots are shown on the left and signal on the right normalized to untreated cells, with a dotted line indicating this base-line.

Figure 4. RADAR/Western Blot Characterization of PARP1-DNA Adducts Induced by 5-aza-dC

(A) Western blot analysis of protein-DNA adducts recovered by RADAR fractionation of K562 cells which were untreated (NT; lane 3) or treated for times indicated with 1 μM 5-aza-dC (D, lanes 4, 5); 1 μM PARPi (BMN-673, B, lanes 6-9); or pretreated with 1 μM 5-aza-dC for 48 hr, at which time PARPi was added and culture continued for indicated times (1, 2 or 18 hr; D/B; lanes 10-12). Whole cell extract, WCE (lane 1); ladder marker, M (lane 2). Blots were probed with anti-full-length recombinant PARP1 (anti-fl-PARP1). Bars on left indicate marker sizes; arrows identify full-length PARP1 in WCE and the apparent 89 kD apoptotic PARP1 fragment in RADAR extracts.
(B) Western blot analysis of adducts isolated from GM639 and K562 cells. Duplicate blots were probed with (left) anti-cc-PARP1, specific for the neo-epitope on caspase-cleaved PARP1; and (right) anti-cat-PARP1, which recognizes an epitope in the catalytic domain. Whole cell extract from cells treated with staurosporine, WCE STS (lane 1); other notations as in panel B. Arrows identify the 89 kD apoptotic PARP1 fragment specifically recognized by anti-cc-PARP1; and both 113 kD full-length PARP1 and 89 kD PARP1 recognized by anti-cat-PARP1.
(C) Western blot analysis of adducts isolated from GM639 cells in three independent experiments (Expt. 1, 2, 3). Notations as in panel B, except that in Expt. 1 cells were pre-treated for 24 hr with 5-aza-dC prior to addition of PARPi for 24 hr (D/B 24/24); and in Expt 2, cells were cultured continuously in both 5-aza-dC and PARPi (D+B) for indicated times. Samples were resolved on a single gel. The resulting blot was first probed with anti-cc-PARP1, then washed but not stripped and probed with anti-DNMT1. Ladder polypeptide sizes indicated between images. Arrow identifies DNMT1.

Figure 5. Working Model for Induction of Cytotoxic PARP1-DNA Adducts by 5-aza-dC or PARPi

PARP1-DNA adducts can form in response to two kinds of DNA damage: (left) spontaneous damage dependent upon PARP1 for repair; or (right) damage induced by 5-aza-dC incorporation,

which causes recruitment of DNMT1 and formation of DNMT1-DNA adducts which may undergo aberrant repair. PARPi treatment may inhibit repair of DNA damage or of PARP1-DNA adducts. PARP1-DNA adducts cause replication arrest and apoptosis. Activated caspases 3, 7 cleave PARP1 to generate adducts bearing the signature neo-epitope identified on PARP1-DNA adducts by RADAR/Western analysis.

SUPPLEMENTARY FIGURE LEGENDS

Figure S1. Dose-response analysis of the effect of 5-aza-dC on viability

Dose-response analysis of viability of four human cell lines treated with 5-aza-dC for 66 hr, quantified by CellTiter-Glo®. Cell lines analyzed were GM639 SV40-transformed fibroblasts; K562 cells, derived from a chronic myelogenous leukemia (CML) patient in blast crisis; HL-60 cells, a promyeolocytic line derived from an AML patient; and CCRF-CEM cells, a T cell line derived from an acute lymphocytic leukemia.

Figure S2. Depletion by siDNMT1 and siPARP1

Western blot of extracts of K562 and GM639 cells treated with siDNMT1 or siPARP1 and probed with antibodies to DNMT1, full-length PARP1 (fl-PARP1), or α-tubulin.

Figure S3. Depletion of DNMT1 does not affect the response to 5-aza-dC; but depletion of PARP1 increases sensitivity to topotecan.

Effect of depletion of DNMT1 or PARP1 on the response of K562 or GM639 cells to drug treatment quantified by CellTiter-Glo® viability assays. Cells were treated for 48 hr with siDNMT1, siPARP1, or non-specific siRNA, siNT2; then cultured for 96 hr with azacytidine (5-aza-C, AZA; 0-4 μM); or for 48 hr with topotecan (0-1 μM).

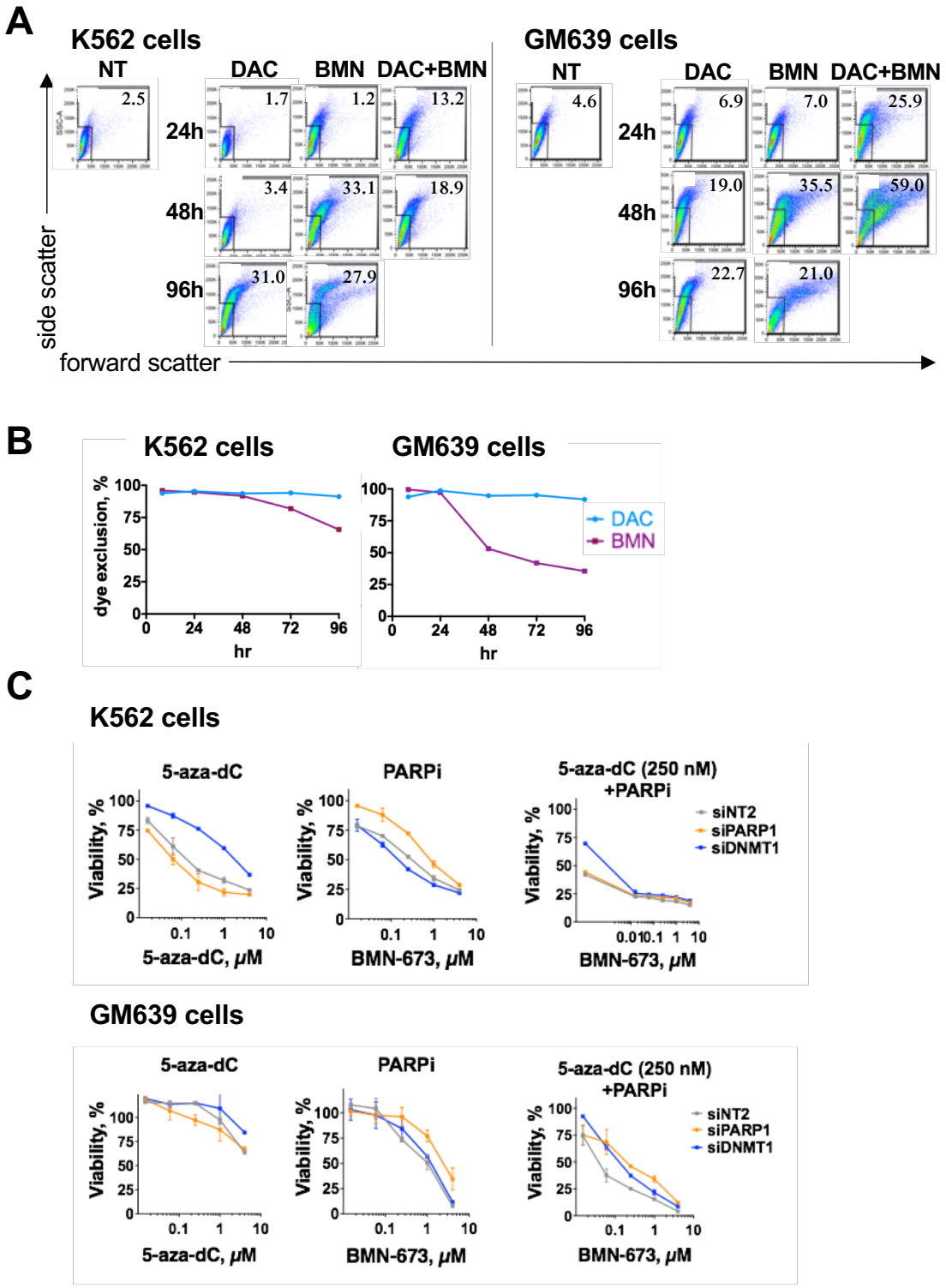
A
K562 cells
NT
DAC
BMN
DAC+BMN
24h
48h
96h
2.5
1.7
1.2
13.2
3.4
33.1
18.9
31.0
27.9
GM639 cells
4.6
6.9
7.0
25.9
19.0
35.5
59.0
22.7
21.0
side scatter
forward scatter
B
K562 cells
GM639 cells
dye exclusion, %
hr
DAC
BMN
C
K562 cells
5-aza-dC
PARPi
5-aza-dC (250 nM) +PARPi
Viability, %
5-aza-dC, μM
BMN-673, μM
siNT2
siPARP1
siDNMT1
GM639 cells

Figure 1

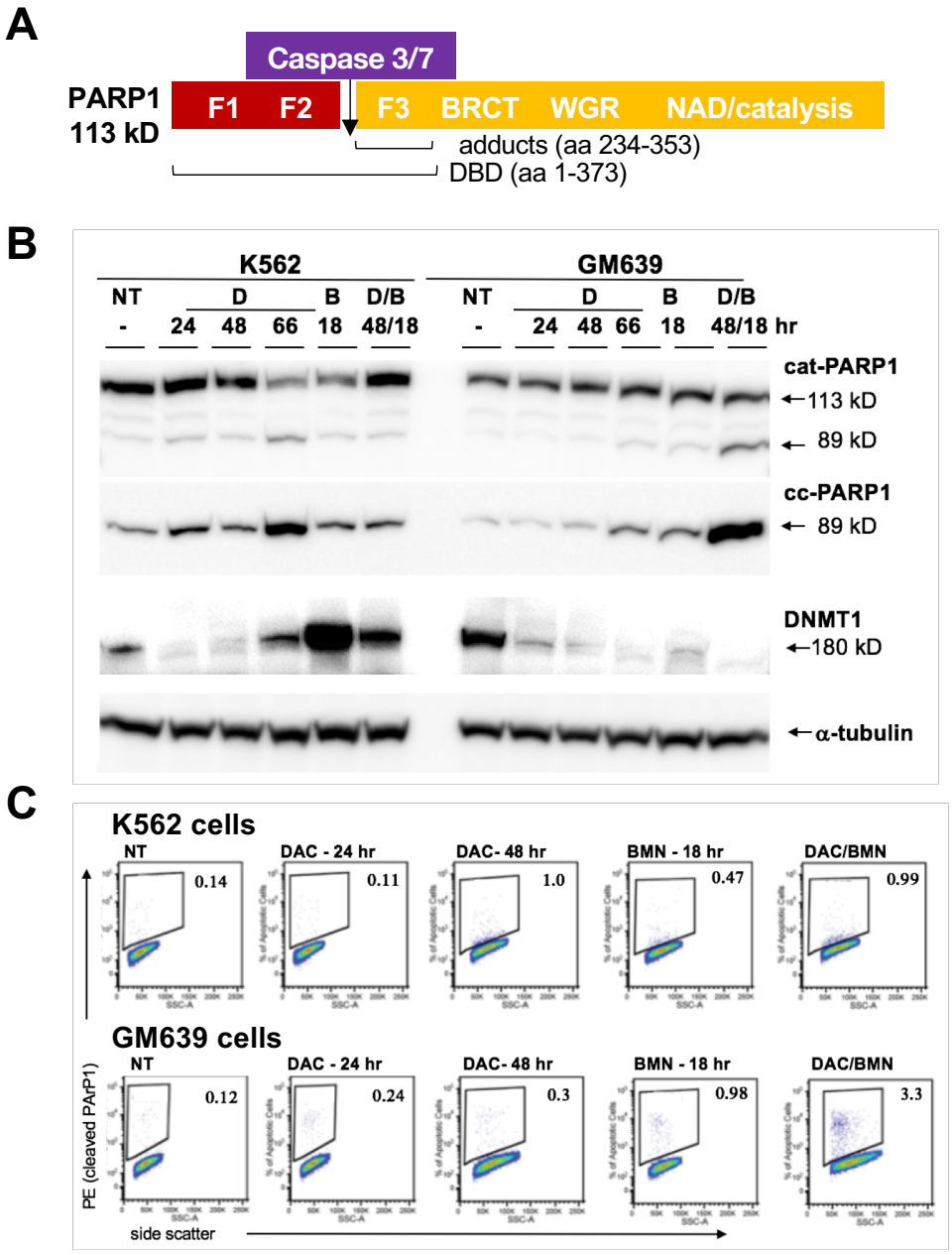
A
Caspase 3/7
PARP1
113 kD
F1
F2
F3
BRCT
WGR
NAD/catalysis
adducts (aa 234-353)
DBD (aa 1-373)
B
K562
GM639
NT
D
B
D/B
-
24
48
66
18
48/18
hr
cat-PARP1
113 kD
89 kD
cc-PARP1
89 kD
DNMT1
180 kD
α-tubulin
C
K562 cells
NT
DAC - 24 hr
DAC- 48 hr
BMN - 18 hr
DAC/BMN
0.14
0.11
1.0
0.47
0.99
GM639 cells
0.12
0.24
0.3
0.98
3.3
PE (cleaved PArP1)
side scatter

Figure 2

A

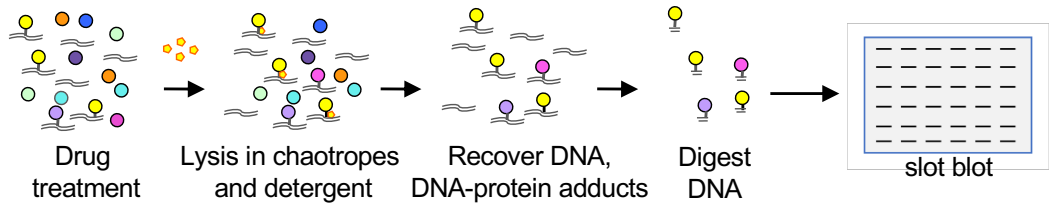

B

PARP1-DNA adducts

K562 cells **GM639 cells**

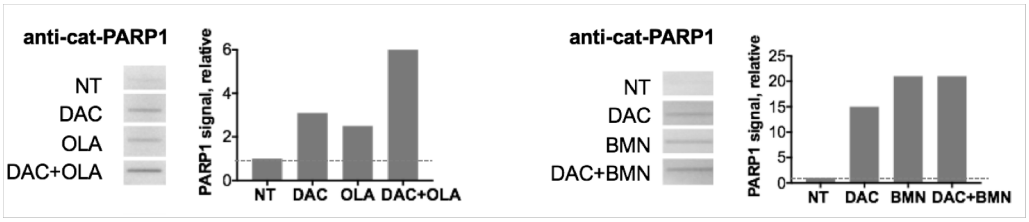

C

DNMT1-DNA adducts

GM639 cells

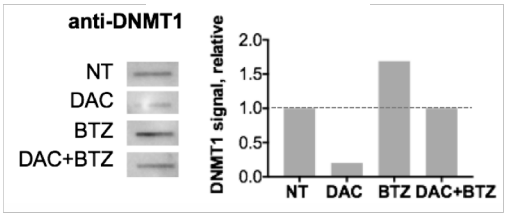

Figure 3

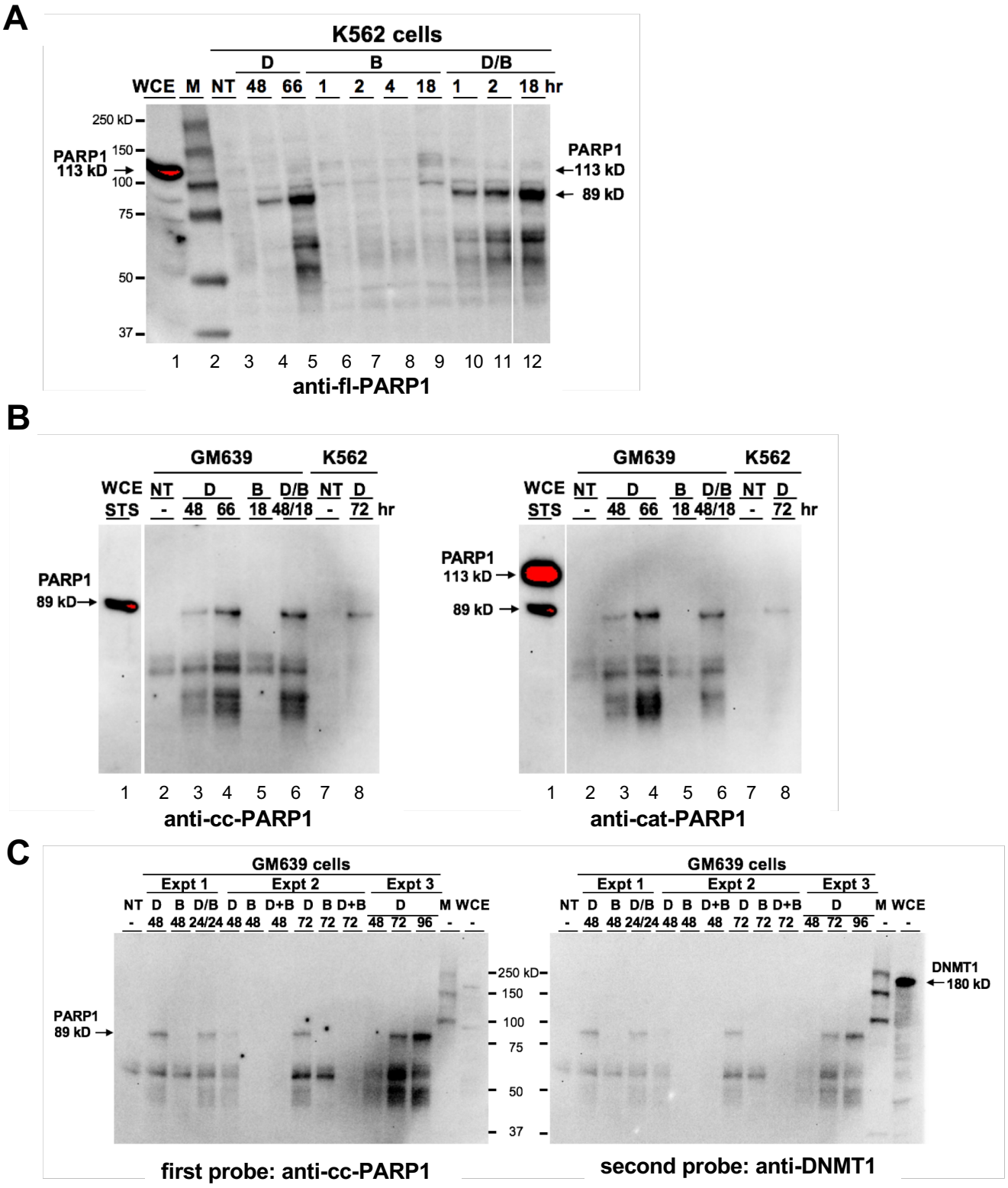
A
K562 cells
D
B
D/B
WCE M NT 48 66 1 2 4 18 1 2 18 hr
250 kD
150
100
75
50
37
PARP1
113 kD
PARP1
113 kD
89 kD
1 2 3 4 5 6 7 8 9 10 11 12
anti-fl-PARP1
B
GM639
K562
WCE NT D B D/B NT D
STS - 48 66 18 48/18 - 72 hr
PARP1
89 kD
1 2 3 4 5 6 7 8
anti-cc-PARP1
GM639
K562
WCE NT D B D/B NT D
STS - 48 66 18 48/18 - 72 hr
PARP1
113 kD
89 kD
1 2 3 4 5 6 7 8
anti-cat-PARP1
C
GM639 cells
Expt 1
Expt 2
Expt 3
NT D B D/B D B D+B D B D+B D M WCE
- 48 48 24/24 48 48 48 72 72 72 48 72 96 - -
PARP1
89 kD
250 kD
150
100
75
50
37
first probe: anti-cc-PARP1
GM639 cells
Expt 1
Expt 2
Expt 3
NT D B D/B D B D+B D B D+B D M WCE
- 48 48 24/24 48 48 48 72 72 72 48 72 96 - -
DNMT1
180 kD
second probe: anti-DNMT1

Figure 4

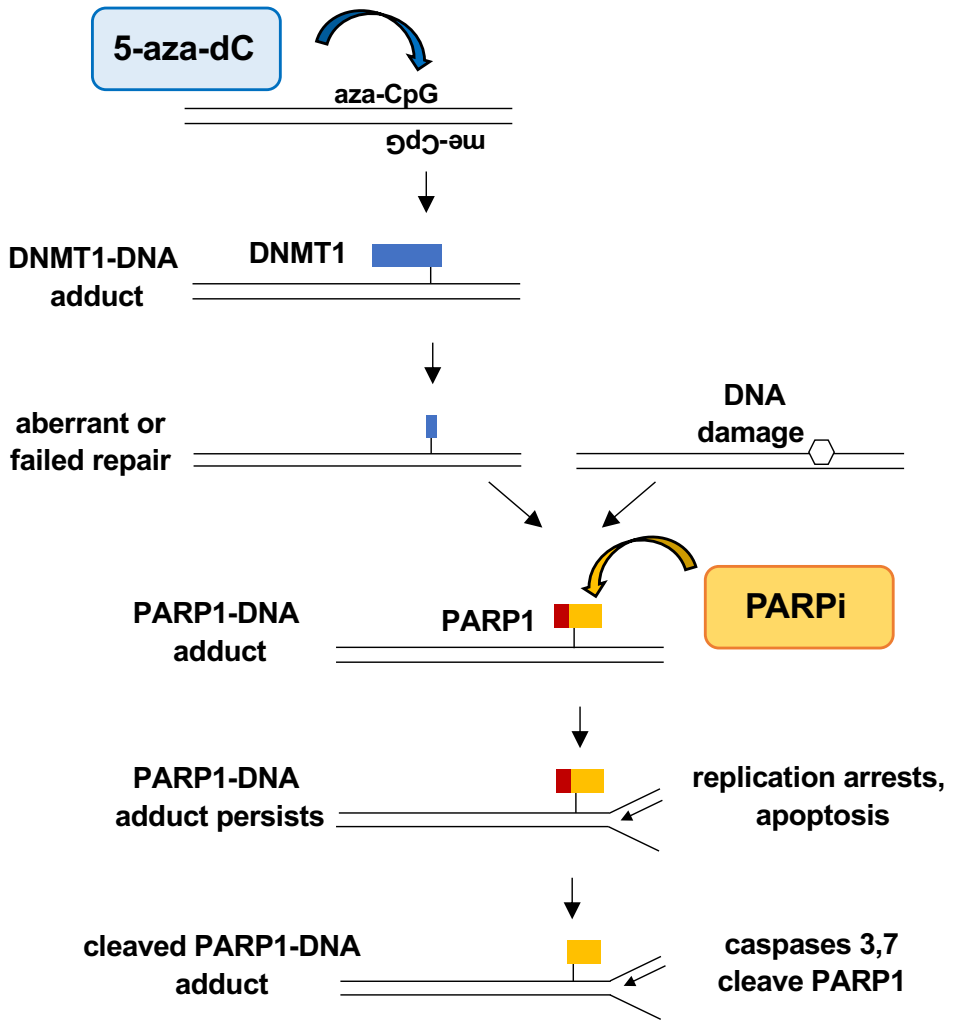
5-aza-dC
aza-CpG
me-CpG
DNMT1-DNA
adduct
DNMT1
aberrant or
failed repair
DNA
damage
PARP1-DNA
adduct
PARP1
PARPi
PARP1-DNA
adduct persists
replication arrests,
apoptosis
cleaved PARP1-DNA
adduct
caspases 3,7
cleave PARP1

Figure 5

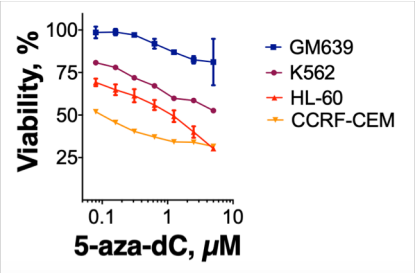
Viability, %
100
75
50
25
0.1
1
10
5-aza-dC, μM
GM639
K562
HL-60
CCRF-CEM

Figure S1

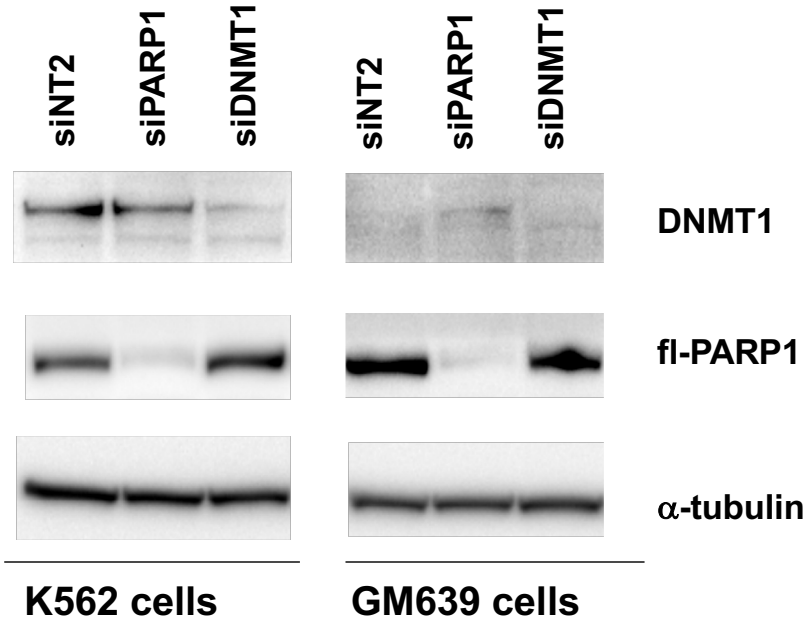
siNT2
siPARP1
siDNMT1
siNT2
siPARP1
siDNMT1
DNMT1
fl-PARP1
α-tubulin
K562 cells
GM639 cells

Figure S2

K562 cells

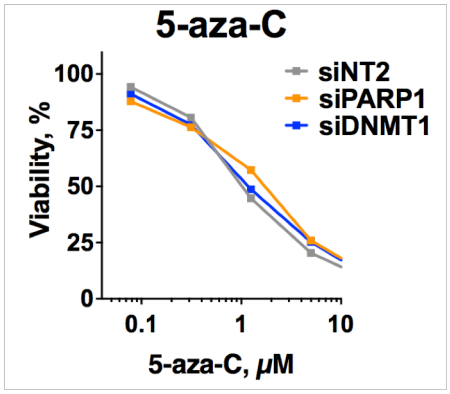

GM639 cells

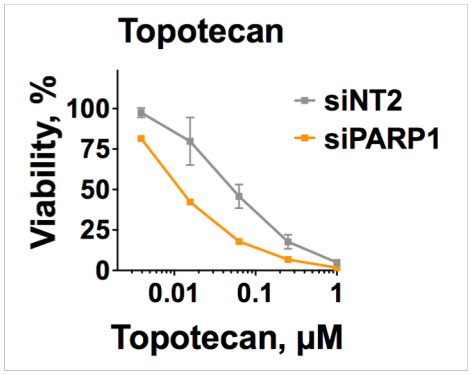

Figure S3